Modeling the Acid-Base Properties of Montmorillonite Edge Surfaces

Christophe Tournassat, James A Davis, Christophe Chiaberge, Sylvain Grangeon, Ian C. Bourg

Modeling the acid-base properties of montmorillonite edge surfaces

Christophe Tournassat[a,b,c*], James A. Davis[b], Christophe Chiaberge[c], Sylvain Grangeon[c], Ian C. Bourg[d]

[a] Université d'Orléans - CNRS/INSU - BRGM, UMR 7327 Institut des Sciences de la Terre d'Orléans, 45071 Orléans, France

[b] Earth and Environmental Sciences Division, Lawrence Berkeley National Laboratory, Berkeley, USA

[c] BRGM, French geological Survey, Orléans, France

[d] Department of Civil and Environmental Engineering and Princeton Environmental Institute, Princeton, USA

[*] corresponding author: c.tournassat@brgm.fr

Abstract

The surface reactivity of clay minerals remains challenging to characterize because of a duality of adsorption surfaces and mechanisms that does not exist in the case of simple oxide surfaces: clay minerals edge surfaces have a variable proton surface charge arising from hydroxyl functional groups, whereas basal surfaces have a permanent negative charge arising from isomorphic substitutions. Hence, the relationship between surface charge and surface potential on edge surfaces cannot be described using the Gouy-Chapman relation, because of a spillover of negative electrostatic potential from the basal surface onto the edge surface. While surface complexation models can be modified to account for these features, a predictive fit of experimental data was not possible until recently, because of uncertainty regarding the densities and intrinsic pK_a values of edge functional groups. Here, we reexamine this problem in light of new knowledge on intrinsic pK_a values obtained over the last decade using *ab initio* molecular dynamics simulations, and we propose a new formalism to describe edge functional groups. Our simulation results yield good predictions of the best available experimental acid-base titration data.

1. Introduction

Clay minerals are natural fine-grained particles, ubiquitous in terrestrial weathering environments, that strongly influence the permeability, mechanics, and pore water chemistry of soils, sediments, and rocks in which they are found [1,2]. In particular, these minerals control the performance of natural and engineered clay barriers used in the isolation of landfills and contaminated sites and proposed for use in the geological storage of high-level radioactive waste [3,4]. A widely examined feature of clay minerals that influences the performance of these barriers

is their cation-exchange capacity, the result of isomorphic substitutions in the structure [5]. In addition to this cation-exchange capacity, clay minerals, including montmorillonite (the most studied swelling clay mineral) carry oxide-type functional groups on their edge surfaces. These oxide-type functional groups, though present in much smaller quantity than the cation exchange sites, dominate the adsorption of trace metals, oxyanions, and organic molecules [6–9], the dissolution and growth kinetics of clay minerals [10,11], and the colloidal mechanics of clay particles [12], at least in some conditions.

In the case of simple oxide minerals, surface reactivity is strongly influenced by their net proton surface charge, which varies with pH through reactions of the following type, where $>SOH_n$ is a generic surface site [13]:

$$> \mathrm{SOH}_n \rightleftarrows > \mathrm{SOH}_{n-1} + \mathrm{H}^+ \quad (1)$$

The reaction described by Eq. (1) gives rise to a variable net proton surface charge density (σ_H) that depends on pH and ionic strength (I, dimensionless[14]). In the case of simple oxide minerals, the last few decades have seen steady advances in the characterization of their proton surface chemistry through a combination of experiments (in particular, acid-base titration and electrophoretic mobility measurements), surface complexation model (SCM) calculations, and bond-valence theory predictions of the intrinsic acidity constants of surface functional groups [15–19]. In the case of the oxide-type functional groups on the montmorillonite edge surfaces, however, σ_H remains poorly understood, as shown by the wide range of reported values of the point of zero net proton charge (p.z.n.p.c., the pH value where $\sigma_H = 0$) and by the variety of models that have been used to describe σ_H [9,20]. As described below, the difficulty in characterizing σ_H on montmorillonite relates to the high permanent structural charge of the solid ($\sigma_0 \approx -1$ $mmol_c \cdot g^{-1}$)

and to the presence of two different surfaces (edge and basal surfaces) with very different properties. These properties have no equivalent in simple oxide minerals, but are widespread features of lamellar structures including vernadite, a phyllomanganate that controls the fate of trace metals in certain oxidized soils and sediments [21,22], green rust, a layered double hydroxide that influences the mobility of iron and anions in reduced soils [23], and synthetic phases widely used in materials chemistry, such as synthetic layered double hydroxides [24].

The challenges associated with characterizing the proton surface reactivity of montmorillonite were summarized a decade ago by Bourg et al. [20]. A first challenge is that montmorillonite particles undergo significant dissolution during acid-base titration measurements. This can be rendered near-negligible in the pH range from about 4.5 to 9.5 through a careful choice of clay pretreatment, storage, and titration procedures[25–29] (see below). Unfortunately, most montmorillonite acid-base titration datasets do not fit the best practices established by Duc et al. [25–28]. A second challenge is that acid-base titration measurements do not directly measure the net proton surface charge density σ_H but rather $\delta\sigma_H$, the *change* in net proton surface charge density relative to its initial value $\sigma_{H,init}$ ($\delta\sigma_H = \sigma_H - \sigma_{H,init}$). Conversion of $\delta\sigma_H$ to σ_H values requires knowledge of $\sigma_{H,init}$ or of the p.z.n.p.c. at the conditions of interest [30]. For simple oxide surfaces, this is achieved by measuring the sum of the adsorbed ion charge densities q_i of all species except H^+ and OH^- (Δq) and applying the charge balance relation [30]:

$$\sigma_0 + \sigma_H + \Delta q = 0 \qquad (2)$$

For montmorillonite, experimental uncertainties make it impossible to accurately determine σ_H using Eq. (2), because σ_H is small compared to σ_0 and Δq [20,29]. Alternatively, the p.z.n.p.c. of oxide surfaces is sometimes determined by assuming that it coincides with the point of zero salt

effect (p.z.s.e., the pH value at which acid-base titration curves carried out at different ionic strengths intersect) or with the isoelectric point (i.e.p., the pH value where the electrophoretic mobility equals zero) [31]. These alternative methods, however, are neither strictly rigorous [20,30] nor applicable to montmorillonite, for which a p.z.s.e. or i.e.p. are not observed [26,32–34]. Finally, the p.z.n.p.c. of montmorillonite is sometimes assumed to correspond to the pH value obtained by adding incremental amounts of dry solid to a solution [35], but this so-called "mass titration" technique, just like a standard acid-base titration, is sensitive to the initial protonation state of the solid [36].

A third challenge arises when attempting to develop a SCM for montmorillonite. An important assumption of SCMs is that the ratio of activity coefficients of different surface species is a function of the surface electrostatic potential ψ. For the reaction described by Eq. (1), the relationship is almost always expressed with a quasi-thermodynamic equilibrium equation of the form:

$$K_{\mathrm{a}} = \frac{[> \mathrm{SOH}_{n-1}](\mathrm{H}^{+})}{[> \mathrm{SOH}_{n}]} \exp\left(\frac{-F\psi}{RT}\right) \qquad (3)$$

where K_{a} is an intrinsic equilibrium constant, (H^{+}) is the thermodynamic activity of H^{+}, square brackets denote mole fractions, ψ is the surface electrostatic potential, F is the Faraday constant (96 485 C mol^{-1}), R is the ideal gas constant (8.314 J mol^{-1} K^{-1}), and T is temperature (in K). Closure of any SCM requires a model of ψ as a function of surface charge, ionic strength, and other conditions. For this, most studies rely on the Gouy-Chapman relation, a mean-field theory prediction based on the Poisson-Boltzmann equation (PBE) of the relationship between surface charge density and surface potential on an infinite planar surface in contact with an ideal electrolyte solution [31,37]. Montmorillonite consists of flake-shaped, 1-nm-thick layers such that

the narrow edge surface cannot be *a priori* treated as an infinite planar surface [9,20]. Solutions to the Poisson-Boltzmann equation for various possible arrangements of the montmorillonite layers indicate that the value of ψ at montmorillonite edges (ψ_{edge}) is influenced by the charge density of both edge and basal surfaces in a manner that depends on ionic strength and on the stacking arrangement of montmorillonite layers [9,20,38]. Finally, a fourth challenge is that montmorillonite edge surfaces carry a variety of functional groups associated with tetrahedral Si and octahedral Al atoms (>SiOH, >AlOH, >Al_2OH, >AlSiOH) as well as additional groups that arise from isomorphic substitutions of Si by Al and of Al by Mg, Fe^{II}, or Fe^{III}. In the absence of independent predictions of the densities and intrinsic acidity constants of each surface functional group, model fits to experimental acid-base titration data are necessarily non-unique [20].

Bourg et al. [20] showed that the first three challenges outlined above could be resolved using information available a decade ago. The second challenge was resolved by using an SCM to predict both $\sigma_{H,init}$ (from reported conditions of clay pre-treatment) and σ_H. The first challenge required identifying experimental datasets that followed that best practices established by Duc et al. [26–28] and that used montmorillonite samples pre-treated by repeated washing in a solution of well-known pH and ionic strength (as required to predict $\sigma_{H,init}$); the available database included only two datasets, those of Baeyens and Bradbury [39] and Duc et al. [27]. The third challenge was resolved by solving a two-dimensional version of the PBE near the edge surface of an isolated montmorillonite particle. The fourth challenge, however, could not be satisfactorily resolved, because of large disagreements between different bond-valence model predictions of the intrinsic pK_a values of edge surface sites [40,41] and, also, because of insufficient knowledge of the densities of different edge surface sites [41]. Eventually, Bourg et al. [20] concluded that experimental data on

121 the acid-base chemistry of montmorillonite edge surfaces could not be predicted from first
122 principles using existing knowledge.

123 The last decade has seen a significant number of new studies of the acid-base surface chemistry
124 of montmorillonite. Several new potentiometric titration studies have been carried out [42–47] as
125 well as one study that attempted to determine the i.e.p. of montmorillonite edge surfaces [48].
126 Several studies have provided new estimates of the edge specific surface area of montmorillonite
127 particles [10,49]. Models of ψ_{edge} have been refined using new Poisson-Boltzmann calculations [9] and
128 Grand Canonical Monte Carlo (GCMC) simulations [50]. Finally, *ab initio* MD simulations have
129 been used to predict the intrinsic pK_a values of montmorillonite edge surface sites [51–57]. Here, we
130 revisit the conclusions of Bourg et al. [20] in light of these advances. First, we show that new
131 knowledge obtained during the last decade provides a more coherent picture of the proton surface
132 chemistry of montmorillonite. Then, we develop a state-of-the-art SCM for montmorillonite edge
133 surfaces, and we note possibilities for future improvements. This new SCM is mainly based on a
134 combination of the existing 2D Poisson-Boltzmann calculations, which are representative of clay
135 edges geometry, with the development of a revised thermodynamic concept for the description of
136 the edge sites, and with the use of pK_a values that have been obtained from *ab initio* MD
137 simulations.

138 ## 2. Constraints on the proton surface chemistry of montmorillonite edges

139 ### 2.1. Montmorillonite edge structure

140 Current knowledge of the densities of different types of montmorillonite edge functional groups
141 remains limited by uncertainty regarding edge crystallographic orientations. Crystal growth
142 theory calculations, surface Coulomb energy considerations, atomistic simulations, and *in situ*

observation of dissolution kinetics using atomic force microscopy suggest the that most stable edge surfaces are perpendicular to [010] and [110] (or, equivalently, [$\bar{1}$10]) [58–63], where the Miller indices are assigned according to Churakov [60] (Figure 1). The two edge surfaces are sometimes referred to as the B and AC edges, respectively, following the seminal study by White and Zelazny [63]. Recent molecular dynamics (MD) and *ab initio* MD simulations of hydrated clay edges suggest that the surface normal to [110] may be significantly more stable than the surface normal to [010] in the presence of liquid water [61,62,64].

Montmorillonite edge surfaces are routinely assumed to have the same stoichiometry and structure as the bulk crystal, with minor bond-length relaxation to accommodate over- or under-coordinated surface O atoms [40]. Recent MD and *ab initio* MD simulation results reveal a more complex picture, the most well-established finding being that cations in the octahedral layer can adopt a five-fold coordination [55,61,65,66].

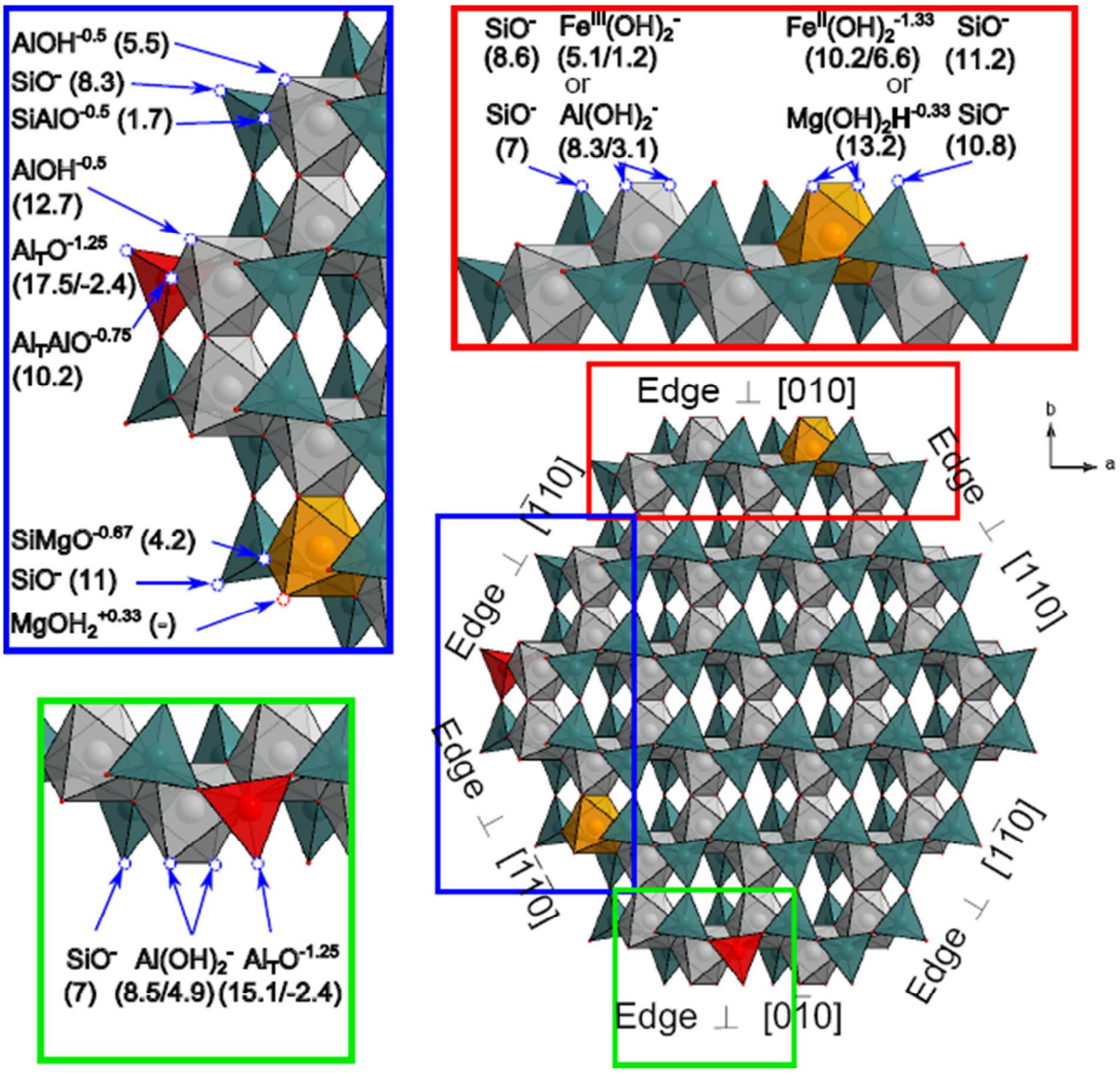

155

156 Figure 1. Edge surface sites of a model montmorillonite particle. Inserts with red and green
157 borders describe sites on the B edge. The insert with a blue border describes sites on the AC
158 edge. The clay mineral structure was taken from Viani et al. [67] and is representative of the
159 structures considered in bond valence calculations and *ab initio* MD simulations. Grey octahedra:
160 Al or Fe(III); orange octahedra: Mg or Fe(II); green tetrahedra: Si; red tetrahedra: Al. Isomorphic
161 substitutions are only shown if they occur at the edge surface. The stoichoimetries of the
162 deprotonated sites are written on the figure along with numbers corresponding to the log *K* values

of the associated protonation reactions predicted by *ab initio* MD calculations (see Section 2.4; an absence of value means that the site does not protonate/deprotonate in the pH range 1 to 14).

2.2. Edge specific surface area

An important parameter in studies of montmorillonite edge reactivity is the edge specific surface area, $a_{s,edge}$. Unfortunately, the N_2 gas adsorption method with the Brunauer-Emmett-Teller technique (N_2-BET) quantifies only the external surface area of crystals (stacks of montmorillonite layers) after drying, which provides no information on $a_{s,edge}$ [68]. The ethylene glycol monoethyl ether (EGME) adsorption method quantifies the total specific surface area of montmorillonite layers, a_s, dominated by the basal surfaces [69]. In principle, $a_{s,edge}$ equals the difference between the measured a_s value and the theoretical basal specific surface area $a_{s,basal}$ [≈ 750 to 780 $m^2\ g^{-1}$ [70]]. Unfortunately, EGME-derived a_s values show a significant dependence on experimental conditions [68] that precludes a precise calculation of $a_{s,edge}$.

Direct measurements of $a_{s,edge}$ for montmorillonite have been achieved using two approaches. The first consists in evaluating edge specific surface area by statistical analysis of particle morphology from atomic force microscopy (AFM) or transmission electron microscopy (TEM) images [71–73]. Alternatively, the derivative isotherms summation (DIS) method distinguishes different clay surfaces in a single gas adsorption measurement based on differences in adsorption energy [68]. Comparison of microscopic imaging and DIS results yields satisfactory agreement (Table S-1), with a possible slight overestimation of edge surface area by the DIS method [74].

2.3. Edge surface electrostatic potential

As noted above, SCMs of proton adsorption on montmorillonite require a model of the edge surface electrostatic potential, ψ_{edge}. Most modeling studies have assumed that clay edges do not develop a significant electrostatic potential ($\psi_{edge} = 0$) [41,75–79] or that ψ_{edge} follows the Gouy-Chapman relation for an infinite planar surface [33,35,43,80–91]. The few studies that solved the PBE near clay edges for realistic geometries, however, showed that ψ_{edge} differs strongly from zero and from the Gouy-Chapman model prediction and is sensitive to the stacking arrangement of the clay layers [38,92–94]. Bourg et al. [20] solved a two-dimensional form of the PBE near the edge surface of an isolated montmorillonite layer (consistent with exfoliated layers in Na-montmorillonite suspensions at ionic strengths lower than I~0.2) and found that ψ_{edge} was reasonably described by:

$$\frac{F\psi_{edge}}{RT} = A_1 \operatorname{asinh}\left(A_2\left(Q_{edge} + A_3\right)\right) \quad (4)$$

where Q_{edge} (C·m^{-2}) is the charge at the edge and A_1 (unitless), A_2 (m^{-2}·C) and A_3 (C·m^{-2}) are parameters that were fitted with the ψ_{edge} values obtained from the full resolution of the 2D PB equation. For montmorillonite at 25 °C, Tournassat et al. [9] refined the values of these parameters to: A_1 = 1.4 -1.2 log I, A_2 = 11 + log I, and A_3 = -0.02 × (-log I)$^{1.60}$. This equation can be compared with the classical Gouy-Chapman model for infinite planar surfaces [13]:

$$\frac{F\psi}{RT} = 2\operatorname{asinh}(B \cdot \sigma) \text{ with } B = \frac{1}{\sqrt{8\varepsilon\varepsilon_0 RT \cdot 1000 \cdot I}} \quad (5)$$

where σ is the surface charge density (in m^{-2}). A key prediction of Eq. 4 is that ψ_{edge} is negative when the edge surface charge is zero (Figure 2) because of a spillover of negative electrostatic potential from the basal surfaces [92,94].

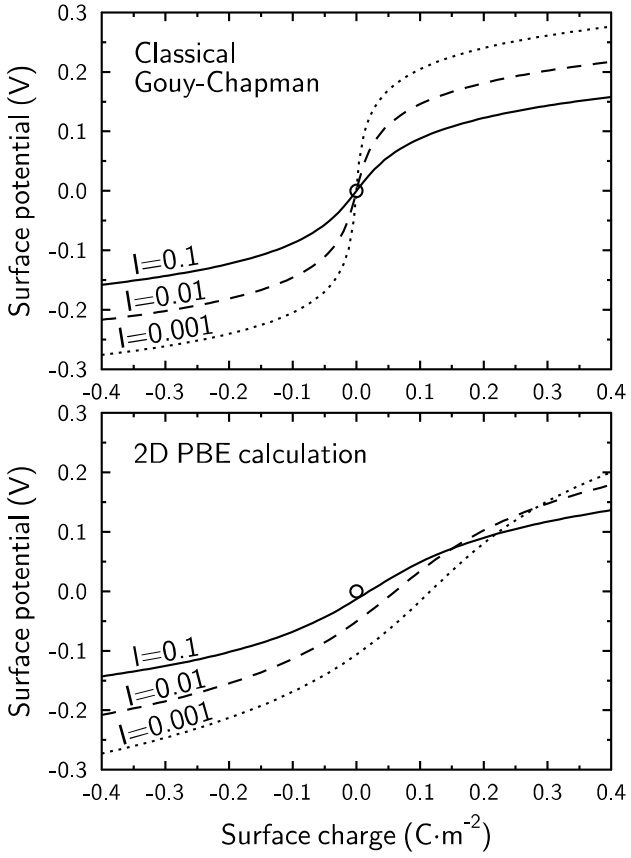

Figure 2. Comparison of the relationships between surface charge (horizontal axis) and surface electrostatical potential (vertical axis) predicted by the classical Gouy-Chapman model for a flat oxide surface (top) and by the PBE calculations of Bourg et al. [20] for the edge surface of an isolated montmorillonite layer (bottom) at three ionic strengths. The circles mark the condition of zero charge and zero potential on each graph.

A potential limitation to the accuracy of the PBE is that it uses the mean-field theory approximation, i.e., it neglects specific ion-ion and ion-surface site interactions. On infinite flat

surfaces, the PBE is nevertheless known to adequately predict the structure of the electrical double layer except at high salinities or in the presence of multivalent counterions [37,95,96]. In the case of montmorillonite, an opportunity to verify the validity of Eq. (4) is provided by GCMC simulations of the acid-base chemistry of individual clay particles where water was treated as a uniform dielectric continuum [50]. To this end, we implemented Eq. (4) in PHREEQC [97] (the modification of the source code is made available in the supporting information file; a executable file can be sent upon request) and predicted the protonation of surface sites using the same site densities and pK_a values as Delhorme et al. [50] (PHREEQC scripts and database are available in the supporting information file). An excellent agreement was found between the two predictions (Figure 3), suggesting that Eq. (4) is valid over the entire range of experimental conditions where montmorillonite particles are made of single layers. This condition is met in experiments carried out with montmorillonite particles dispersed in a NaCl or $NaClO_4$ background electrolyte at ionic strengths lower than I~0.2 [98–101].

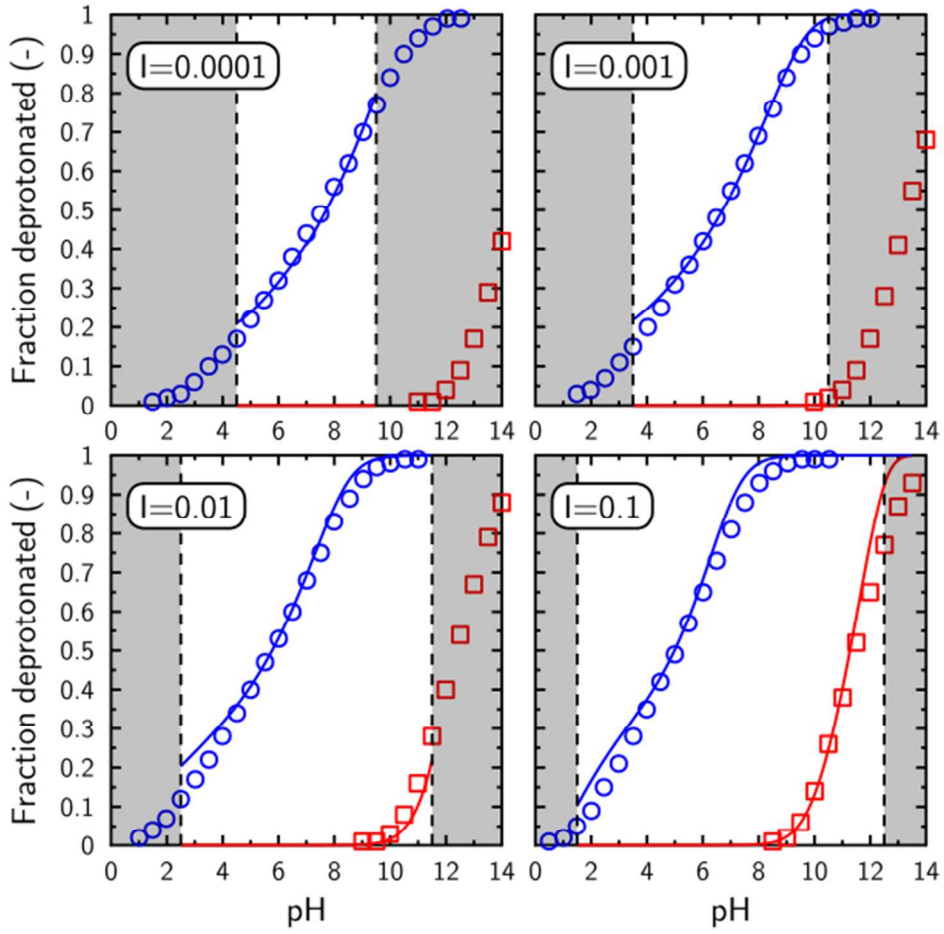

Figure 3. Comparison of the GCMC simulations of Delhorme et al. [50] (circles and squares) with an SCM that used Eq. (4) (solid lines) at three different ionic strengths in NaCl salt background. Both models used the same site densities and intrinsic pK_a values. Activity coefficients of solute species in the SCM were modeled using the extended Debye-Hückel formalism. Blue symbols and lines refer to aluminol sites having a pK_a of 3.75 and a site density of 4.5 nm^{-2}; red symbols and lines refer to silanol sites having a pK_a of 8.0 and a site density of 5.2 nm^{-2}. Shaded areas correspond to conditions that cannot exist, i.e., domains where the specified ionic strength is exceeded because of high H^+ or OH^- concentrations.

2.4. Intrinsic pK_a values of edge surface sites

Until recently, theoretical estimates of the intrinsic pK_a values of edge surface sites were based on bond-valence theories. The resulting predicted pK_a values were highly sensitive to model assumptions [40,41] and did not provide accurate predictions of experimental montmorillonite titration data [20]. In the last decade, *ab initio* MD simulations have proved capable of accurately predicting the intrinsic pK_a values of simple oxide surface functional groups [102–104], including oxide-type functional groups on montmorillonite edge surfaces [51–57]. In particular, a series of papers by Liu et al. [51–55] explored the influence of edge crystallographic orientation and the presence of octahedral and tetrahedral substitutions on the intrinsic pK_a values of edge surface groups. Their predictions are summarized in Figure 1. It is noteworthy that similar sites on the surfaces perpendicular to the [010] and [110] crystallographic directions have different reactivity according to the *ab initio* MD calculations. For example, silanol sites (>SiOH) have pK_a values of 7.0 on the [010] edge vs. 8.3 on the [110] edge when no octahedral substitution is present. These values are significantly different from the values predicted by bond valence methods [40,41] and used by Bourg et al. [20] (Table S-2).

2.5. Experimental data

Duc et al. [26–28] carried out a comprehensive examination of montmorillonite acid-base titration methodologies and identified a series of best practices. These included careful montmorillonite pre-treatment and storage procedures (use of a series of acid washes at pH ≈ 4, exchangeable cation homogenization at ionic strength $I \approx 1$, and rinsing steps; storage in liquid water at low temperature for relatively short durations, or storage of freeze-dried samples as an acceptable alternative). For the titration experiments themselves, they noted the importance of using an inert atmosphere and limiting the experiments to the pH range ≈ 4.5-9.5. They found that a continuous

titration method was acceptable if equilibration times between additions of acid or base were short (< 10 min) and if hysteresis was quantified; alternatively, a discontinuous batch titration method was acceptable if the atoms released by clay dissolution (Si, Al, Mg, Fe) were analyzed (both in solution and on the clay cation-exchange sites) to account for pH buffering by side reactions. In the alkaline domain, however, correction of the raw batch titration data for measured side reactions failed to reproduce the continuous titration curves. The authors concluded on the superiority of fast, continuous methods for quantifying the dissociable surface charge of clays. Among the many reported studies of montmorillonite titration [12,27–29,33–35,39,80,84,86,88–90,105], Bourg et al. [20] determined that only three studies [27,28,39] followed this set of best practices. One of these studies used the batch titration technique [39], and its results at alkaline pH values are therefore of unclear reliability. Of the acid-base titration studies published over the last decade [42–47], none followed the entire established set of best practices while also reporting the pH and ionic strength of the solutions used during clay pre-treatment. The present study, therefore, focuses on the dataset from Duc et al. [27] as the best available set of montmorillonite acid-base titration results.

An interesting indirect quantification of edge surface charge was pursued by Pecini and Avena [48], who measured the i.e.p. of montmorillonite loaded with cationic dyes with a strong affinity for the basal surface. Under the assumption that the dyes completely screen the basal surface charge but do not interact with the edge surfaces (such that the measured i.e.p. reflects edge surface properties) and within the well-established theoretical limitations associated with relating an i.e.p. to a point of zero charge [30], the results of Pecini and Avena [48] suggest that the point of zero charge of clay edge surfaces (the pH value where $\sigma_{0,edge} + \sigma_H = 0$, where $\sigma_{0,edge}$ corresponds to the permanent structural charge density "expressed" on the edge surface) is in the pH range 3.8–5.5, in qualitative agreement with a previous measurement of the i.e.p. of thermally treated Cu-

montmorillonite for which the structural layer charge was reduced to almost zero, whereby the authors estimated that the edge surfaces are negatively charged at pH > 3.5 [106].

3. Towards a predictive SCM for montmorillonite edge surfaces

3.1. Reactivity of edge surface functional groups

To determine whether the new knowledge summarized above allows a predictive simulation of the acid-base chemistry of montmorillonite, we developed a generic SCM for the [010] and [110] edge surfaces in our modified version of PHREEQC that applies Eq. (4) for the calculation of ψ_{edge}. Edge surface functional groups were modeled as groups of one octahedral and two tetrahedral cations together with their associated OH groups. The overall charge of a group was calculated from bond valence principle applied to the terminal oxygen atoms of the edge sites. For example, a fully-deprotonated functional group with no isomorphic substitution on the [010] edge corresponds to the grouping of two Si-O^- sites and one Al-$(OH)_2^-$ site and is denoted >Si-Al-SiO_4^{-3} (leaving the unreactive H out of the formula). It can be protonated four times with intrinsic pK_a values of 8.3, 7, 7, and 3.1 as predicted by *ab initio* MD simulation (section 2.4 and Figure 1). This representation deviates from the classical description used in SCMs, where each surface hydroxyl is modeled as a distinct functional group with a single pK_a value [107]. The advantages of the present representation are that the calculation of the number of sites affected by neighboring substitutions is straightforward and that future implementation of metal adsorption through the formation of multi-dentate surface complexes is made easier with regards to the calculation of surface site activities [9,108]. Simple cases were used to verify that the grouping of surface sites had little effect on model predictions (Fig. SI-1 in supporting information; PHREEQC script files are also available in order to test further the effect of grouping sites). The fractions of edge functional

groups that include octahedral or tetrahedral substitutions were calculated from the structural formula of montmorillonite with the assumption that edge chemistry reflects that of the bulk mineral. Because of the absence of *ab initio* MD simulation predictions of the reactivity of Fe-substituted sites on the [110] edge surface, sites with Fe(III) for Al substitutions on this surface were assigned the same properties as sites without substitutions, while sites with Fe(II) for Al substitutions were assigned the same properties as sites with Mg for Al substitutions. Surface site densities were estimated from crystallographic considerations and from reported clay unit cell formulae: each site group, SiAlSi, AlAlSi, SiMgSi, $SiFe^{III}Si$, and $SiFe^{II}Si$ had a density of 2.06 × x_i nm^{-2}, where $x_{>Si-Mg-Si} = \left(\frac{Mg}{Al+Mg+Fe^{II}+Fe^{III}}\right)_{oct}$, $x_{>Si-Fe^{III}-Si} = \left(\frac{Fe^{III}}{Al+Mg+Fe^{II}+Fe^{III}}\right)_{oct}$, $x_{>Si-Fe^{II}-Si} = \left(\frac{Fe^{II}}{Al+Mg+Fe^{II}+Fe^{III}}\right)_{oct}$, $x_{>Al-Al-Si} = 2 \times \left(\frac{Al}{Si+Al}\right)_{tet}$, and $x_{>Si-Al-Si} = 1 - x_{>Si-Mg-Si} - x_{>Al-Al-Si} - x_{>Si-Fe^{III}-Si} - x_{>Si-Fe^{II}-Si}$. This calculation implicitly neglects the possible existence of edge sites with both octahedral and tetrahedral substitutions or with two tetrahedral substitutions, for which predicted pK_a values are not available.

3.2. Impact of clay permanent structural charge

Proton adsorption by Na-H cation exchange on basal surfaces was taken into account by using a constant selectivity coefficient of 3.2 (log K = 0.5) in near agreement with previously published values [41,109]. The permanent structural charge was set to 0.9 $mol_c \cdot kg^{-1}$, yielding an overall charge density of σ_0 = -0.12 $C \cdot m^{-2}$ for the clay layers. As noted above, the edge surface charge equals $\sigma_{0,edge} + \sigma_H = 0$, where $\sigma_{0,edge}$ is the edge surface charge density resulting from nearby isomorphic substitutions. Bourg et al. [20] assumed that $\sigma_{0,edge} = \sigma_0$ for simplicity. Here, we modeled edge surface charge arising from near-edge isomorphic substitutions in an even simpler way: we added -1 to the valence of edge functional groups that include an isomorphic substitution of Al for Si or

of Mg or Fe(II) for Al. For example, a fully-deprotonated edge functional group with no isomorphic substitutions (>Si-Al-SiO_4^{-3}), upon substitution of Mg for Al, becomes (>Si-Mg-SiO_4^{-4}).

3.3. Predicted acid-base properties of edge surfaces

According to the predictive model described above, montmorillonite edge surface charge has little dependence on the type and extent of layer structural substitutions, but it depends significantly on crystallographic orientation between the [010] and [110] edge surfaces (Figure 4, top). In the presence of 0.1 mol·L^{-1} NaCl, the [010] surface is positively charged at pH < 5, whereas the [110] surface is positively charged only at pH < 3.5, consistent with the experimental findings of Thomas et al. [106] and Pecini and Avena [48]. The relative proportion of [010] and [110] edge surface orientations on montmorillonite is unfortunately unknown, which leaves one unavoidable free parameter in the presently developed SCM.

Changes in ionic strength are predicted to have a marked effect on surface charge but not on the shape of the charge vs. pH curves, especially for the surface perpendicular to [110] (Figure 4, bottom). A decrease in ionic strength results primarily in a translation of the surface charge curve towards higher pH values, in agreement with experimental results.

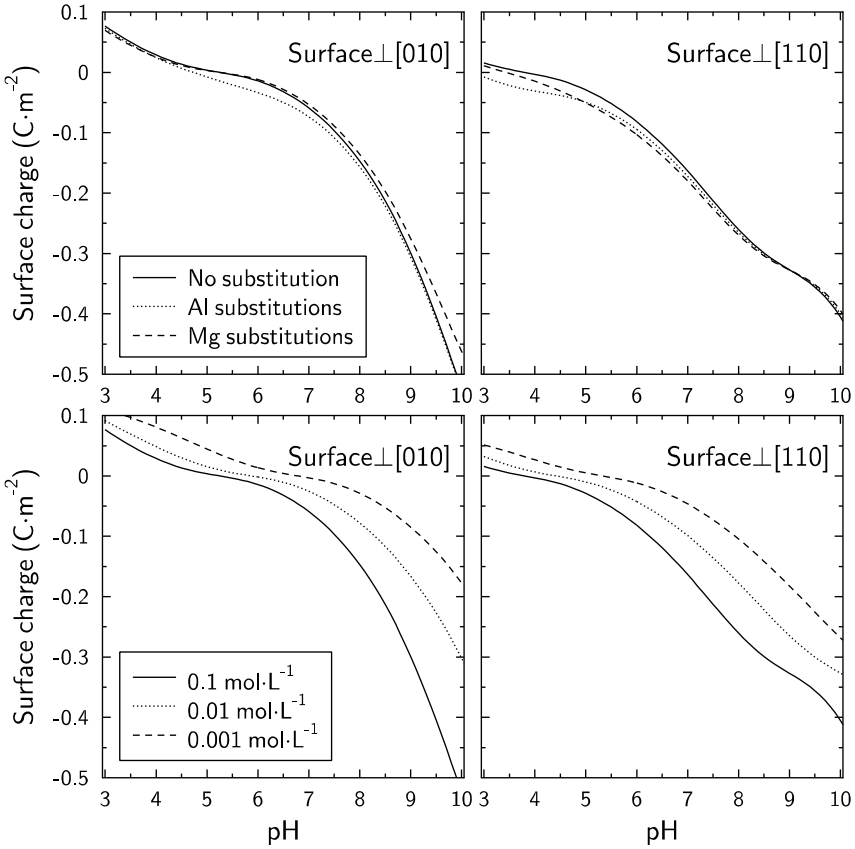

Figure 4. Top: Predicted edge surface charge as a function of pH for montmorillonite particles immersed in a 0.1 mol·L^{-1} NaCl background electrolyte. "No", "Al" and "Mg" substitutions refer to simulations carried out with ($x_{>\mathrm{Si-Mg-Si}} = 0$; $x_{>\mathrm{Al-Al-Si}} = 0$), ($x_{>\mathrm{Si-Mg-Si}} = 0$; $x_{>\mathrm{Al-Al-Si}} = 0.1$) and ($x_{>\mathrm{Si-Mg-Si}} = 0.2$; $x_{>\mathrm{Al-Al-Si}} = 0$) respectively. Bottom: Influence of NaCl concentration (0.001, 0.01, and 0.1 mol·L^{-1}) on the predictions obtained if x>Si-Al-Si = 1.

3.4. Comparison with potentiometric titration data

Model predictions were compared with the potentiometric titration results of Duc et al. [27] for the SWy-2 and MX80 reference montmorillonites (the dataset for SWy-2 was made available in Delhorme et al. [50]). The structural formulae of SWy-2 and MX80 montmorillonites were reported as $(Si_{3.87}Al_{0.13})(Al_{1.52}Mg_{0.25}Fe^{III}_{0.224}Fe^{II}_{0.006})Na_{0.39}O_{10}(OH)_2$ and

$(Si_4)(Al_{1.57}Mg_{0.25}Fe^{III}_{0.09}Fe^{II}_{0.09})Na_{0.34}O_{10}(OH)_2$, respectively [27]. Reported montmorillonite structural formulae can vary as a function of sample preparation and calculation method [65]. This variability adds a minor source of uncertainty to our model predictions according to Figure 4. The $x_{>Si-Mg-Si}$, $x_{>Si-Fe^{II}-Si}$, $x_{>Si-Fe^{III}-Si}$ and $x_{>Al-Al-Si}$ values were set, respectively, to 0.125, 0.045, 0.045 and 0 for MX80 montmorillonite and to 0.125, 0.003, 0.112 and 0.13 for SWy-2 montmorillonite.

A good agreement was found between experimental and predicted potentiometric titration data for SWy-2 montmorillonite if the specific edge surface area was set to 14 $m^2 \cdot g^{-1}$ and the relative abundance of [010] and [110] edges was set to 1:1 (Figure 5). The modeled edge specific surface area is in agreement with the value of 19.2 $m^2 \cdot g^{-1}$ measured on the sample used for the titration experiment (Table S-1), because the DIS method tends to overestimate the surface area [74]. A lesser agreement was found for the lowest ionic strength (I=0.001) at pH values greater than 8, but the significance of this discrepancy is tempered by the increased experimental uncertainty at pH > 9 [20]. For MX80 montmorillonite, the agreement between experimental and predicted potentiometric titration curves was acceptable if the specific edge surface area was set to 12 $m^2 \cdot g^{-1}$ and the relative abundance of [010] and [110] edges was set to 1:1 (Figure 5) (the effect of varying the relative abundance of [010] and [110] edges can be seen on Figure 4, and it can be quantified by using the PHREEQC script files provided in the supporting information). The modeled edge specific surface area was larger than the measured value (Table S-1, from 6 to 9 $m^2 \cdot g^{-1}$, depending on the considered study). However, the values reported in Table S-1 were not measured for the same samples used in the titration experiments. For both titration datasets, the pH values corresponding to $\delta\sigma_H = 0$ were correctly predicted at all investigated ionic strengths. A better agreement with the experimental data likely could have been achieved by adjusting the

372 pK_a values of edge surface sites in the limit of the uncertainty reported in Liu et al. [51–55] (from
373 ± 0.6 to ± 1.6 depending on the site under consideration), but such a refinement was not deemed
374 justified in light of the uncertainties in the experimental data. Such exercise can be done using the
375 files made available in the supporting information.

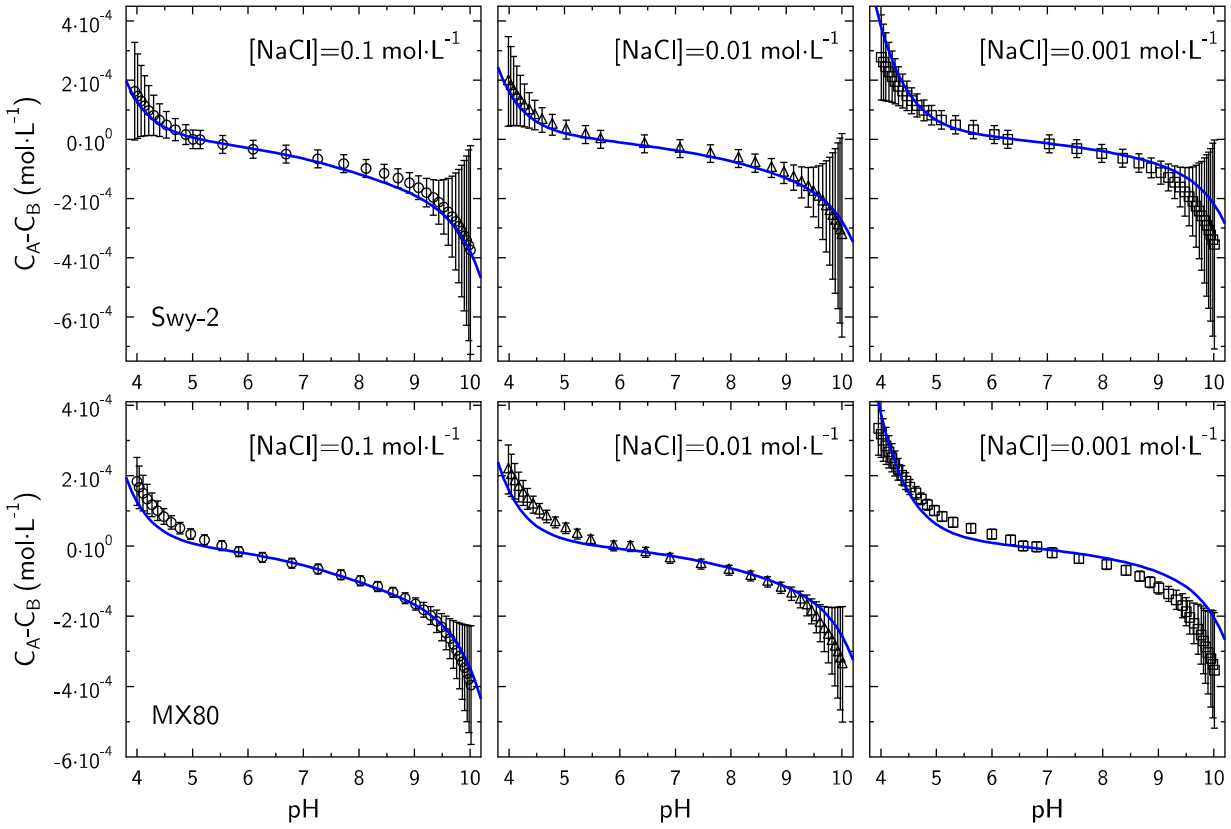

376

377 Figure 5. Comparison of model predictions (lines) and potentiometric titration data (symbols[27,50])
378 for MX80 montmorillonite (bottom) and SWy-2 montmorillonite (top). The specific edge surface
379 area was set to 12 $m^2 \cdot g^{-1}$ and 14 $m^2 \cdot g^{-1}$ for MX80 and Swy-2 montmorillonite respectively, and
380 the relative abundance of [010] and [110] edges was set at 0.5/0.5. Error bands were estimated as
381 in Bourg et al. [20].

The present study relies on several simplifying assumptions or conditions that inherently limit the range of applicability of the proposed model. First and foremost, the model was derived for the case of simple indifferent 1:1 electrolytes such as NaCl at relatively dilute concentrations (≤ 0.1 M) where clay layer stacking is minimal and where the mean field approximation inherent in the PBE is valid. Extension of the model to a broader set of conditions would require a new model of ψ_{edge} derived for the appropriate aggregation structure of montmorillonite layers and for deviations from the mean-field approximation. A significant challenge to such an extension is that the best-quality experimental titration data are limited to the conditions modeled in the present study.

Another important condition for the applicability of our proposed model is that the model's description of edge surface sites must be accurate. At the most fundamental level, this condition can be challenged on the grounds that most, if not all, theoretical calculations of montmorillonite edge site properties were carried out based on a pyrophillite-like model structure, which is *trans*-vacant, whereas available data suggest that most montmorillonites have a *cis*-vacant structure [110,111]. Structural OH groups have different positions in *cis*- and *trans*-vacant structures. Additionally, *cis*-vacant structures are not centrosymmetric [111], and the types of edge surface configurations are thus more diverse than for *trans*-vacant structures. In particular, edge surface site configurations are different for the edges perpendicular to the [010] and $[0\bar{1}0]$ crystallographic directions in a *cis*-vacant structure, whereas they are the same in a *trans*-vacant structure (see Figure S-1 in supporting information).

4. Acknowledgement

This work was supported by the French Radioactive Waste Management Agency (Andra) in the framework of the Andra-BRGM scientific partnership (CTEC project). J.A.D. acknowledges funding from L'Institut Carnot for his visit to the BRGM and from the U.S. Department of Energy under Contract DE-AC02-05CH11231 under the auspices of the Office of Nuclear Energy, Used Fuel Disposition program. I.C.B. was supported by the U.S. Department of Energy under Contract DE-AC02-05CH11231 through the Office of Science, Office of Basic Energy Sciences, Geosciences program.

5. TOC

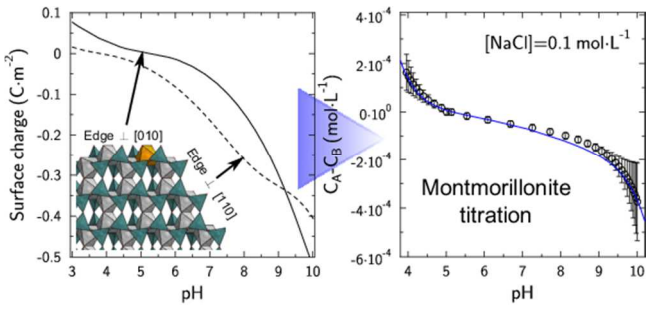

6. References

(1) Bourg, I. C. Sealing shales versus brittle shales: A sharp threshold in the material properties and energy technology uses of fine-grained sedimentary rocks. *Env. Sci. Tech. Lett.* **2015**, *2*, 255–259.

(2) Tournassat, C.; Bourg, I. C.; Steefel, C. I.; Bergaya, F. Introduction; In *Natural and Engineered Clay Barriers*; Tournassat, C.; Steefel, C. I.; Bourg, I. C.; Bergaya, F., Eds.; Developments in Clay Science; Elsevier, 2015; Vol. 6, pp. 1–4.

(3) Borisover, M.; Davis, J. A. Chapter 2 - Adsorption of inorganic and organic solutes by clay minerals; In *Natural and Engineered Clay Barriers*; Tournassat, C.; Steefel, C. I.; Bourg, I. C.; Bergaya, F., Eds.; Developments in Clay Science; Elsevier, 2015; Vol. 6, pp. 33–70.

(4) Bourg, I. C.; Tournassat, C. Chapter 6 - Self-diffusion of water and ions in clay barriers; In *Natural and Engineered Clay Barriers*; Tournassat, C.; Steefel, C. I.; Bourg, I. C.; Bergaya, F., Eds.; Developments in Clay Science; Elsevier, 2015; Vol. 6, pp. 71–100.

(5) Bourg, I. C.; Sposito, G. Ion exchange phenomena; In *Handbook of Soil Science, second edition*; Huang, P. M.; Li, Y.; Sumner, M. E., Eds.; CRC Press: Boca Raton, 2011.

(6) Manning, B. A.; Goldberg, S. Adsorption and stability of arsenic(III) at the clay mineral-water interface. *Env. Sci. Tech.* **1997**, *31*, 2005–2011.

(7) Schlegel, M. L.; Manceau, A. Evidence for the nucleation and epitaxial growth of Zn phyllosilicate on montmorillonite. *Geochim. Cosmochim. Acta* **2006**, *70*, 901–917.

(8) Strawn, D. G.; Sparks, D. L. The use of XAFS to distinguish between inner-and outer-sphere lead adsorption complexes on montmorillonite. *J. Colloid Interface Sci.* **1999**, *216*, 257–269.

(9) Tournassat, C.; Grangeon, S.; Leroy, P.; Giffaut, E. Modeling specific pH dependent sorption of divalent metals on montmorillonite surfaces. A review of pitfalls, recent achievements and current challenges. *Am. J. Sci.* **2013**, *313*, 395–451.

(10) Marty, N. C. M.; Cama, J.; Sato, T.; Chino, D.; Villiéras, F.; Razafitianamaharavo, A.; Brendlé, J.; Giffaut, E.; Soler, J. M.; Gaucher, E. C.; Tournassat, C. Dissolution kinetics of synthetic Na-smectite. An integrated experimental approach. *Geochim. Cosmochim. Acta* **2011**, *75*, 5849–5864.

(11) Yang, L.; Steefel, C. I. Kaolinite dissolution and precipitation kinetics at 22 °C and pH 4. *Geochim. Cosmochim. Acta* **2008**, *72*, 99–116.

(12) Tombácz, E.; Szekeres, M. Surface charge heterogeneity of kaolinite in aqueous suspension in comparison with montmorillonite. *Appl. Clay Sci.* **2006**, *34*, 105–124.

(13) Davis, J. A.; James, R. O.; Leckie, J. O. Surface ionization and complexation at the oxide/water interface: I. Computation of electrical double layer properties in simple electrolytes. *J. Colloid Interface Sci.* **1978**, *63*, 480–499.

(14) Solomon, T. The definition and unit of ionic strength. *J. Chem. Educ.* **2001**, *78*, 1691–1692.

(15) Bickmore, B. R.; Tadanier, C. J.; Rosso, K. M. New approach for predicting acidity constants: Combining bond-valence and ab initio methods. *Abstracts of Papers of the American Chemical Society* **2004**, *227*, U1203–U1203.

(16) Goldberg, S.; Criscenti, L. J. Modeling adsorption of metals and metalloids by soil components; In *Biophysico-chemical processes of heavy metals and metalloids in soil environments*; Violante, A.; Huang, P. M.; Gadd, G. M., Eds.; John Wiley & Sons, Hoboken, N J, 2008; pp. 215–264.

(17) Machesky, M. L.; Predota, M.; Wesolowski, D. J.; Vlcek, L.; Cummings, P. T.; Rosenqvist, J.; Ridley, M. K.; Kubicki, J. D.; Bandura, A. V.; Kumar, N.; Sofo, J. O. Surface protonation at the rutile (110) interface: explicit incorporation of solvation structure within the refined MUSIC model framework. *Langmuir* **2008**, *24*, 12331–12339.

(18) Sposito, G. Characterization of particle surface charge; In *Environmental particles*; Buffle, J.; Van Leeuwen, H. P., Eds.; Lewis Publisher, Chelsea, Michigan, USA, 1992; Vol. 1, pp. 291–314.

(19) Sverjensky, D. A.; Sahai, N. Theoretical prediction of single-site surface-protonation equilibrium constants for oxides and silicates in water. *Geochim. Cosmochim. Acta* **1996**, *60*, 3773–3797.

(20) Bourg, I. C.; Sposito, G.; Bourg, A. C. M. Modeling the acid-base surface chemistry of montmorillonite. *J. Colloid Interface Sci.* **2007**, *312*, 297–310.

(21) Bargar, J. R.; Fuller, C. C.; Marcus, M. A.; Brearley, A. J.; Rosa, M. P. De la; Webb, S. M.; Caldwell, W. A. Structural characterization of terrestrial microbial Mn oxides from Pinal Creek, AZ. *Geochim. Cosmochim. Acta* **2009**, *73*, 889–910.

(22) Manceau, A.; Kersten, M.; Marcus, M. A.; Geoffroy, N.; Granina, L. Ba and Ni speciation in a nodule of binary Mn oxide phase composition from Lake Baikal. *Geochim. Cosmochim. Acta* **2007**, *71*, 1967–1981.

(23) Trolard, F.; Bourrié, G.; Abdelmoula, M.; Refait, P.; Feder, F. Fougerite, a new mineral of the pyroaurite-iowaite group: description and crystal structure. *Clays Clay Miner.* **2007**, *55*, 323–334.

(24) Wang, S.-L.; Liu, C. H.; Wang, M. K.; Chuang, Y. H.; Chiang, P. N. Arsenate adsorption by Mg/Al–NO3 layered double hydroxides with varying the Mg/Al ratio. *Appl. Clay Sci.* **2009**, *43*, 79–85.

(25) Duc, M.; Carteret, C.; Thomas, F.; Gaboriaud, F. Temperature effect on the acid-base behaviour of Na-montmorillonite. *J. Colloid Interface Sci.* **2008**, *327*, 472–476.

(26) Duc, M.; Gaboriaud, F.; Thomas, F. Sensitivity of the acid-base properties of clays to the methods of preparation and measurement: 1. Literature review. *J. Colloid Interface Sci.* **2005**, *289*, 139–147.

(27) Duc, M.; Gaboriaud, F.; Thomas, F. Sensitivity of the acid-base properties of clays to the methods of preparation and measurement: 2. Evidence from continuous potentiometric titrations. *J. Colloid Interface Sci.* **2005**, *289*, 148–156.

(28) Duc, M.; Thomas, F.; Gaboriaud, F. Coupled chemical processes at clay/electrolyte interface: A batch titration study of Na-montmorillonites. *J. Colloid Interface Sci.* **2006**, *300*, 616–625.

(29) Tournassat, C.; Greneche, J.-M.; Tisserand, D.; Charlet, L. The titration of clay minerals. Part I. Discontinuous backtitration technique combined to CEC measurements. *J. Colloid Interface Sci.* **2004**, *273*, 224–233.

(30) Sposito, G. On points of zero charge. *Environ. Sci. Technol.* **1998**, *32*, 2815–2819.

(31) Davis, J. A.; Kent, D. Surface complexation modeling in aqueous geochemistry. *Rev. Mineral. Geochem.* **1990**, *23*, 177–260.

(32) Sondi, I.; Biscan, J.; Pravdic, V. Electrokinetics of pure clay minerals revisited. *J. Colloid Interface Sci.* **1996**, *178*, 514–522.

(33) Tertre, E.; Castet, S.; Berger, G.; Loubet, M.; Giffaut, E. Surface chemistry of kaolinite and Na-montmorillonite in aqueous electrolyte solutions at 25 and 60ęgreC: Experimental and modeling study. *Geochim. Cosmochim. Acta* **2006**, *70*, 4579–4599.

(34) Tombácz, E.; Szekeres, M. Colloidal behavior of aqueous montmorillonite suspensions: the specific role of pH in the presence of indifferent electrolytes. *Appl. Clay Sci.* **2004**, *27*, 75–94.

(35) Avena, M. J.; De Pauli, C. Proton adsorption and electrokinetics of an argentinean montmorillonite. *J. Colloid Interface Sci.* **1998**, *202*, 195–204.

(36) Žalac, S.; Kallay, N. Application of mass titration to the point of zero charge determination. *J. Colloid Interface Sci.* **1992**, *149*, 233–240.

(37) Sposito, G. *The surface chemistry of natural particles*; Oxford University Press: New York, 2004; p. 242.

(38) Kraepiel, A. M. L.; Keller, K.; Morel, F. M. M. On the acid-base chemistry of permanently charged minerals. *Env. Sci. Tech.* **1998**, *32*, 2829–2838.

(39) Baeyens, B.; Bradbury, M. H. A mechanistic description of Ni and Zn sorption on Na-montmorillonite. Part I: Titration and sorption measurements. *J. Contam. Hydrol.* **1997**, *27*, 199–222.
(40) Bickmore, B. R.; Rosso, K. M.; Nagy, K. L.; Cygan, R. T.; Tadanier, C. J. Ab initio determination of edge surface structures for dioctahedral 2:1 phyllosilicates: Implications for acid-base reactivity. *Clays Clay Miner.* **2003**, *51*, 359–371.
(41) Tournassat, C.; Ferrage, E.; Poinsignon, C.; Charlet, L. The titration of clay minerals II. Structure-based model and implications for clay reactivity. *J. Colloid Interface Sci.* **2004**, *273*, 234–246.
(42) Bogolepov, A. A. Simulation of U(VI) and Co(II) sorption on montmorillonite. *Radiochemistry (Moscow, Russian Federation)(Translation of Radiokhimiya)* **2009**, *51*, 96–103.
(43) Gu, X. Y.; Evans, L. J.; Barabash, S. J. Modeling the adsorption of Cd(II), Cu(II), Ni(II), Pb(II) and Zn(II) onto montmorillonite. *Geochim. Cosmochim. Acta* **2010**, *74*, 5718–5728.
(44) Korichi, S.; Bensmaili, A. Sorption of uranium (VI) on homoionic sodium smectite experimental study and surface complexation modeling. *J. Hazard. Mater.* **2009**, *169*, 780–793.
(45) Kriaa, A.; Hamdi, N.; Srasra, E. Acid-base chemistry of montmorillonitic and beidellitic-montmorillonitic smectite. *Russ. J. Electrochem.* **2007**, *43*, 167–177.
(46) Rozalén, M.; Brady, P. V.; Huertas, F. J. Surface chemistry of K-montmorillonite: Ionic strength, temperature dependence and dissolution kinetics. *J. Colloid Interface Sci.* **2009**, *333*, 474–484.
(47) Tan, X. L.; Hu, J.; Zhou, X.; Yu, S. M.; Wang, X. K. Characterization of Lin'an montmorillonite and its application in the removal of Ni2+ from aqueous solutions. *Radiochim. Acta* **2008**, *96*, 487–495.
(48) Pecini, E. M.; Avena, M. J. Measuring the isoelectric point of the edges of clay mineral particles: The case of montmorillonite. *Langmuir* **2013**, *29*, 14926–14934.
(49) Le Forestier, L.; Muller, F.; Villiéras, F.; Pelletier, M. Textural and hydration properties of a synthetic montmorillonite compared with a natural Na-exchanged clay analogue. *Appl. Clay Sci.* **2010**, *48*, 18–25.
(50) Delhorme, M.; Labbez, C.; Caillet, C.; Thomas, F. Acid-base properties of 2:1 clays. I. Modeling the role of electrostatics. *Langmuir* **2010**, *26*, 9240–9249.
(51) Liu, X.; Cheng, J.; Sprik, M.; Lu, X.; Wang, R. Interfacial structures and acidity of edge surfaces of ferruginous smectites. *Geochim. Cosmochim. Acta* **2015**, *168*, 293–301.
(52) Liu, X.; Cheng, J.; Sprik, M.; Lu, X.; Wang, R. Surface acidity of 2:1-type dioctahedral clay minerals from first principles molecular dynamics simulations. *Geochim. Cosmochim. Acta* **2014**, *140*, 410–417.
(53) Liu, X.; Lu, X.; Cheng, J.; Sprik, M.; Wang, R. Temperature dependence of interfacial structures and acidity of clay edge surfaces. *Geochimica et Cosmochimica Acta* **2015**, *160*, 91–99.
(54) Liu, X.; Lu, X.; Sprik, M.; Cheng, J.; Meijer, E. J.; Wang, R. Acidity of edge surface sites of montmorillonite and kaolinite. *Geochim. Cosmochim. Acta* **2013**, *117*, 180–190.
(55) Liu, X. D.; Lu, X. C.; Meijer, E. J.; Wang, R. C.; Zhou, H. Q. Atomic-scale structures of interfaces between phyllosilicate edges and water. *Geochim. Cosmochim. Acta* **2012**, *81*, 56–68.

563 (56) Liu, X. D.; Lu, X. C.; Wang, R. C.; Meijer, E. J.; Zhou, H. Q.; He, H. P. Atomic scale
564 structures of interfaces between kaolinite edges and water. *Geochim. Cosmochim. Acta*
565 **2012**, *92*, 233–242.
566 (57) Tazi, S.; Rotenberg, B.; Salanne, M.; Sprik, M.; Sulpizi, M. Absolute acidity of clay edge
567 sites from ab-initio simulations. *Geochim. Cosmochim. Acta* **2012**, *94*, 1–11.
568 (58) Bickmore, B. R.; Bosbach, D.; Hochella, M. F. J.; Charlet, L.; Rufe, E. In situ atomic
569 force microscopy study of hectorite and nontronite dissolution: implications for
570 phyllosilicate edge surface structures and dissolution mechanisms. *Am. Mineral.* **2001**,
571 *86*, 411–423.
572 (59) Bleam, W. F.; Welhouse, G. J.; Janowiak, M. A. The surface Coulomb energy and proton
573 Coulomb potentials of pyrophyllite {010},{110},{100}, and {130} edges. *Clays Clay*
574 *Miner.* **1993**, *41*, 305–316.
575 (60) Churakov, S. V. Ab initio study of sorption on pyrophyllite: Structure and acidity of the
576 edge sites. *J. Phys. Chem. B* **2006**, *110*, 4135–4146.
577 (61) Newton, A. G.; Kwon, K. D.; Cheong, D.-K. Edge structure of montmorillonite from
578 atomistic simulations. *Minerals* **2016**, *6*, 25.
579 (62) Newton, A. G.; Sposito, G. Molecular dynamics simulations of pyrophyllite edge
580 surfaces: structure, surface energies, and solvent accessibility. *Clays Clay Miner.* **2015**,
581 *63*, 277–289.
582 (63) White, G. N.; Zelazny, L. W. Analysis and implications of the edge structure of
583 dioctahedral phyllosilicates. *Clays Clay Miner.* **1988**, *36*, 141–146.
584 (64) Kwon, K. D.; Newton, A. G. Structure and stability of pyrophyllite edge surfaces: Effect
585 of temperature and water chemical potential. *Geochim. Cosmochim. Acta* **2016**, *190*,
586 100–114.
587 (65) Hadi, J.; Tournassat, C.; Ignatiadis, I.; Greneche, J.-M.; Charlet, L. Modelling CEC
588 variations versus structural iron reduction levels in dioctahedral smectites. Existing
589 approaches, new data and model refinements. *J. Colloid Interface Sci.* **2013**, *407*, 397–
590 409.
591 (66) Lammers, L. N.; Bourg, I. C.; Okumurad, M.; Kolluria, K.; Sposito, G.; Machidad, M.
592 Molecular dynamics simulations of cesium adsorption on illite nanoparticles. *J. Colloid*
593 *Interface Sci.* **2016**, *submitted*,.
594 (67) Viani, A.; Gualtieri, A. F.; Artioli, G. The nature of disorder in montmorillonite by
595 simulation of X-ray powder patterns. *Am. Mineral.* **2002**, *87*, 966–975.
596 (68) Michot, L. J.; Villiéras, F. Chapter 2.10 - Surface Area and Porosity; In *Handbook of*
597 *Clay Science*; Bergaya, F.; Lagaly, G., Eds.; Developments in Clay Science; Elsevier,
598 2013; Vol. 5, pp. 319–332.
599 (69) Srodon, J.; McCarty, D. K. Surface area and layer charge of smectite from CEC and
600 EGME/H_2O-retention measurements. *Clays Clay Miner.* **2008**, *56*, 155–174.
601 (70) Tournassat, C.; Appelo, C. A. J. Modelling approaches for anion-exclusion in compacted
602 Na-bentonite. *Geochim. Cosmochim. Acta* **2011**, *75*, 3698–3710.
603 (71) Cadene, A.; Durand-Vidal, S.; Turq, P.; Brendle, J. Study of individual Na-
604 montmorillonite particles size, morphology, and apparent charge. *J. Colloid Interface*
605 *Sci.* **2005**, *285*, 719–730.
606 (72) Nadeau, P. H. The physical dimensions of fundamental clay particles. *Clay Miner.* **1985**,
607 *20*, 499–514.

608 (73) Tournassat, C.; Neaman, A.; Villiéras, F.; Bosbach, D.; Charlet, L. Nanomorphology of
609 montmorillonite particles: Estimation of the clay edge sorption site density by low-
610 pressure gas adsorption and AFM observations. *Am. Mineral.* **2003**, *88*, 1989–1995.
611 (74) Reinholdt, M. X.; Hubert, F.; Faurel, M.; Tertre, E.; Razafitianamaharavo, A.; Francius,
612 G.; Prêt, D.; Petit, S.; Béré, E.; Pelletier, M.; Ferrage, E. Morphological properties of
613 vermiculite particles in size-selected fractions obtained by sonication. *Appl. Clay Sci.*
614 **2013**, *77*, 18–32.
615 (75) Bradbury, M. H.; Baeyens, B. A mechanistic description of Ni and Zn sorption on Na-
616 montmorillonite. Part II: modeling. *J. Contam. Hydrol.* **1997**, *27*, 223–248.
617 (76) Grambow, B.; Fattahi, M.; Montavon, G.; Moisan, C.; Giffaut, E. Sorption of Cs, Ni, Pb,
618 Eu(III), Am(III), Cm, Ac(III), Tc(IV), Th, Zr, and U(VI) on MX80 bentonite: an
619 experimental approach to assess model uncertainty. *Radiochim. Acta* **2006**, *94*, 627–636.
620 (77) Montavon, G.; Alhajji, E.; Grambow, B. Study of the interaction of Ni^{2+} and Cs^{+} on MX-
621 80 bentonite; Effect of compaction using the "capillary method. *Environ. Sci. Technol.*
622 **2006**, *40*, 4672–4679.
623 (78) Tertre, E.; Beaucaire, C.; Coreau, N.; Juery, A. Modelling Zn(II) sorption onto clayey
624 sediments using a multi-site ion-exchange model. *Appl. Geochem.* **2009**, *24*, 1852–1861.
625 (79) Wolthers, M.; Charlet, L.; Tournassat, C. Reactivity of bentonite. An additive model
626 applied to uranyl sorption; In *Surface complexation modelling*; Lützenkirchen, J., Ed.;
627 Elsevier, 2006.
628 (80) Avena, M. J. Acid-base behavior of clay surfaces in aqueous media. *Encyclopedia of*
629 *surface and colloid science* **2002**, 37–63.
630 (81) Avena, M. J.; Mariscal, M. M.; De Pauli, C. P. Proton binding at clay surfaces in water.
631 *Appl. Clay Sci.* **2003**, *24*, 3–9.
632 (82) Barbier, F.; Duc, G.; Petit-Ramel, M. Adsorption of lead and cadmium ions from
633 aqueous solution to the montmorillonite/water interface. *Colloid. Surface. A.* **2000**, *166*,
634 153–159.
635 (83) Charlet, L.; Schindler, P. W.; Spadini, L.; Furrer, G.; Zysset, M. Cation adsorption on
636 oxides and clays: the aluminum case. *Aquatic Science* **1993**, *55*, 1015–1621.
637 (84) Ikhsan, J.; Wells, J. D.; Johnson, B. B.; Angove, M. J. Surface complexation modeling of
638 the sorption of Zn(II) by montmorillonite. *Colloid. Surface. A.* **2005**, *252*, 33–41.
639 (85) Kowal-Fouchard, A.; Drot, R.; Simoni, E.; Ehrhardt, J. J. Use of spectroscopic
640 techniques for uranium(VI)/montmorillonite interaction modeling. *Env. Sci. Tech.* **2004**,
641 *38*, 1399–1407.
642 (86) Madrid, L.; Diaz-Barrentios, E. Description of titration curves of mixed materials with
643 variable and permanent surface charge by amathematical model. 1. Theory. 2.
644 Application to mixtures of lepidocrocite and montmorillonite. *Journal of Soil Science*
645 **1988**, *39*, 215–225.
646 (87) Marcussen, H.; Holm, P. E.; Strobel, B. W.; Hansen, H. C. B. Nickel sorption to goethite
647 and montmorillonite in presence of citrate. *Env. Sci. Tech.* **2009**, *43*, 1122–1127.
648 (88) Stadler, M.; Schindler, P. W. Modeling of H^{+} and Cu^{2+} adsorption on calcium-
649 montmorillonite. *Clays Clay Miner.* **1993**, *41*, 288–296.
650 (89) Tombácz, E.; Nyilas, T.; Libor, Z.; Csanaki, C. Surface charge heterogeneity and
651 aggregation of clay lamellae in aqueous suspensions; In *Progress in Colloid and Polymer*
652 *Science: From Colloids to Nanotechnology*; Kremer, F.; Lagaly, G., Eds.; Springer,
653 2004; Vol. 125, pp. 206–215.

(90) Wanner, H.; Albinson, Y.; Karnland, O.; Wieland, E.; Wersin, P.; Charlet, L. The acid/base chemistry of montmorillonite. *Radiochim. Acta* **1994**, *66/67*, 157–162.
(91) Zachara, J. M.; Smith, S. C. Edge complexation reactions of cadmium on specimen and soil-derived smectite. *Soil Sci. Soc. Am. J.* **1994**, *58*, 762–769.
(92) Chang, F. R. C.; Sposito, G. The electrical double layer of a disked-shaped clay mineral particle: effect of electrolyte properties and surface charge density. *J. Colloid Interface Sci.* **1996**, *178*, 555–564.
(93) Chang, F. R. C.; Sposito, G. The electrical double layer of a disked-shaped clay mineral particle: effect of particle size. *J. Colloid Interface Sci.* **1994**, *163*, 19–27.
(94) Secor, R. B.; Radke, C. J. Spillover of the diffuse double layer on montmorillonite particles. *J. Colloid Interface Sci.* **1985**, *103*, 237–244.
(95) Henderson, D.; Boda, D. Insights from theory and simulation on the electrical double layer. *Phys. Chem. Chem. Phys.* **2009**, *11*, 3822–3830.
(96) Tinnacher, R. M.; Holmboe, M.; Tournassat, C.; Bourg, I. C.; Davis, J. A. Ion adsorption and diffusion in smectite: molecular, pore, and continuum scale views. *Geochim. Cosmochim. Acta* **2016**, *177*, 130–149.
(97) Parkhurst, D. L.; Appelo, C. A. J. *Description of input and examples for PHREEQC Version 3– a computer program for speciation,batch-reaction, one-dimensional transport, and inverse geochemical calculations*; U.S. Geological Survey Techniques and Methods, book 6, chap. A43, 497 p., available at http://pubs.usgs.gov/tm/06/a43/, 2013.
(98) Méring, J. On the hydration of montmorillonite. *Transaction of Faraday Society* **1946**, *42*, B205–B219.
(99) Norrish, K. The swelling of montmorillonite. *Faraday Discuss. Chem. Soc.* **1954**, *18*, 120–134.
(100) Segad, M.; Hanski, S.; Olsson, U.; Ruokolainen, J.; Åkesson, T.; Jönsson, B. Microstructural and swelling properties of Ca and Na montmorillonite:(in situ) observations with cryo-TEM and SAXS. *J. Phys. Chem. C.* **2012**, *116*, 7596–7601.
(101) Sposito, G. The diffuse-ion swarm near smectite particles suspended in 1:1 electrolyte solutions: modified Gouy-Chapman theory and quasicrystal formation; In *Clay water interface and its rheological implications*; Güven, N.; Pollastro, R. M., Eds.; Clay minerals society, 1992; Vol. 4, pp. 127–156.
(102) Leung, K.; Criscenti, L. J. Predicting the acidity constant of a goethite hydroxyl group from first principles. *J. Phys.: Condens. Matter* **2012**, *24*, 124105.
(103) Leung, K.; Nielsen, I. M.; Criscenti, L. J. Elucidating the bimodal acid-base behavior of the water-silica interface from first principles. *J. Am. Chem. Soc.* **2009**, *131*, 18358–18365.
(104) Sulpizi, M.; Gaigeot, M.-P.; Sprik, M. The silica–water interface: how the silanols determine the surface acidity and modulate the water properties. *J. Chem. Theory Comput.* **2012**, *8*, 1037–1047.
(105) Helmy, A.; Ferreiro, E.; De Bussetti, S. Cation exchange capacity and condition of zero charge of hydroxy-A1 montmorillonite. *Clays Clay Miner.* **1994**, *42*, 444–450.
(106) Thomas, F.; Michot, L. J.; Vantelon, D.; Montarges, E.; Prelot, B.; Cruchaudet, M.; Delon, J. F. Layer charge and electrophoretic mobility of smectites. *Colloid. Surface. A.* **1999**, *159*, 351–358.

(107) Hiemstra, T.; Van Riemsdijk, W. H. On the relationship between charge distribution, surface hydration, and the structure of the interface of metal hydroxides. *J. Colloid Interface Sci.* **2006**, *301*, 1–18.
(108) Kulik, D. A. Thermodynamic concepts in modeling sorption at the mineral-water interface. *Rev. Mineral. Geochem.* **2009**, *70*, 125–180.
(109) Fletcher, P.; Sposito, G. The chemical modeling of clay/electrolyte interactions for montmorillonite. *Clay Miner.* **1989**, *24*, 375–391.
(110) Drits, V. A.; Zviagina, B. B. Trans-vacant and cis-vacant 2:1 layer silicates: structural features, identification, and occurrence. *Clays Clay Miner.* **2009**, *57*, 405–415.
(111) Tsipursky, S. I.; Drits, V. A. The distribution of octahedral cations in the 2:1 layers of dioctahedral smectites studied by oblique-texture electron diffraction. *Clay Miner.* **1984**, *19*, 177–193.

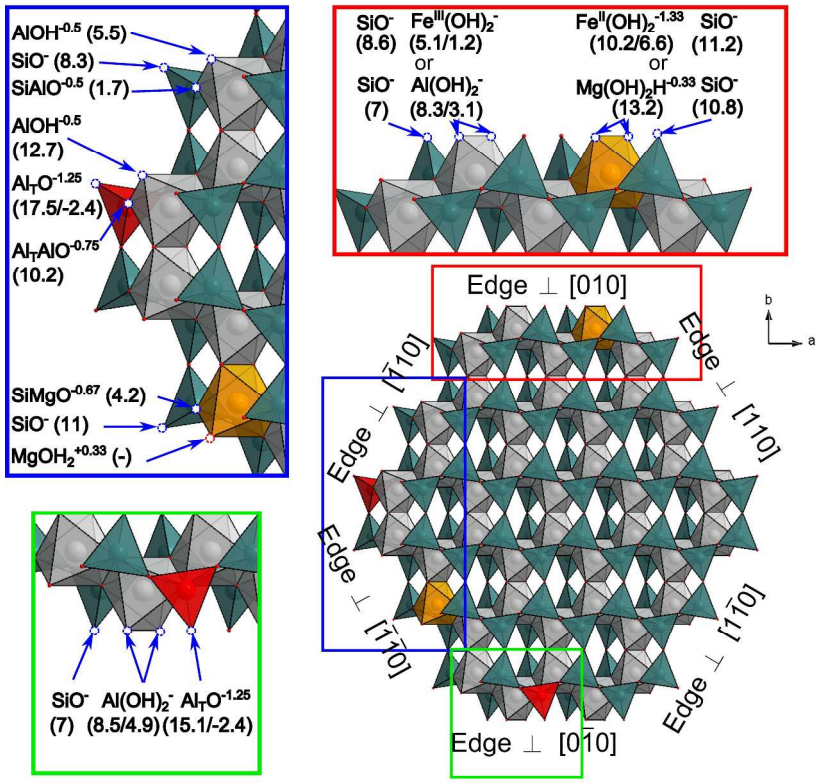

Figure 1

297x420mm (300 x 300 DPI)

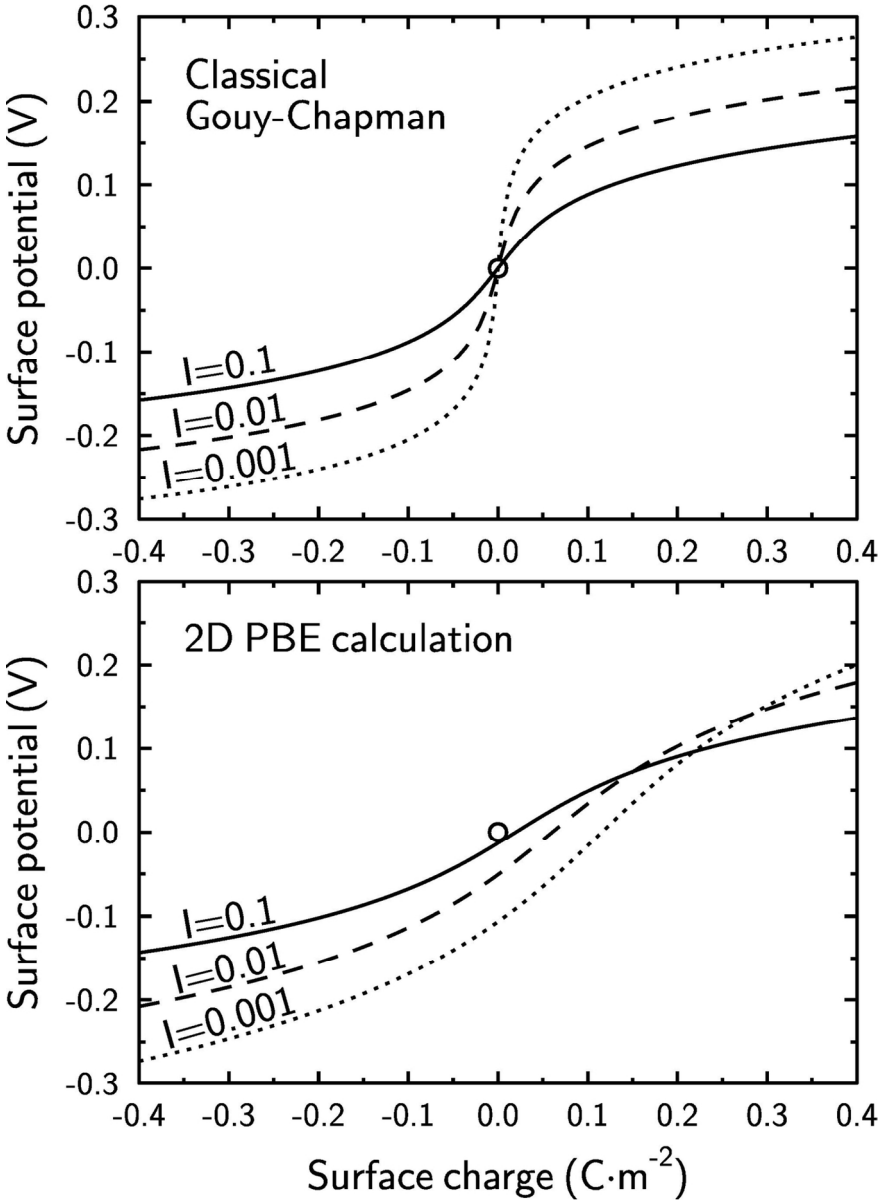

Figure 2

117x161mm (300 x 300 DPI)

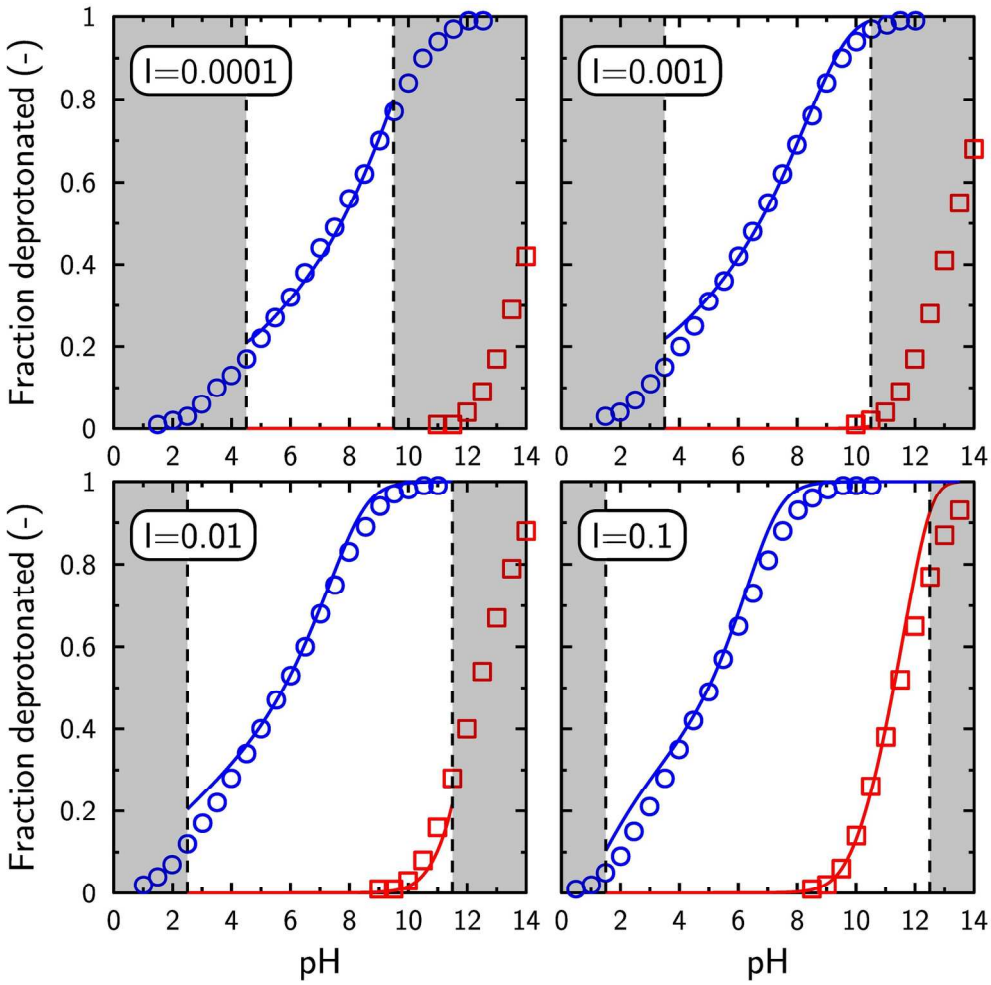

Figure 3

166x163mm (300 x 300 DPI)

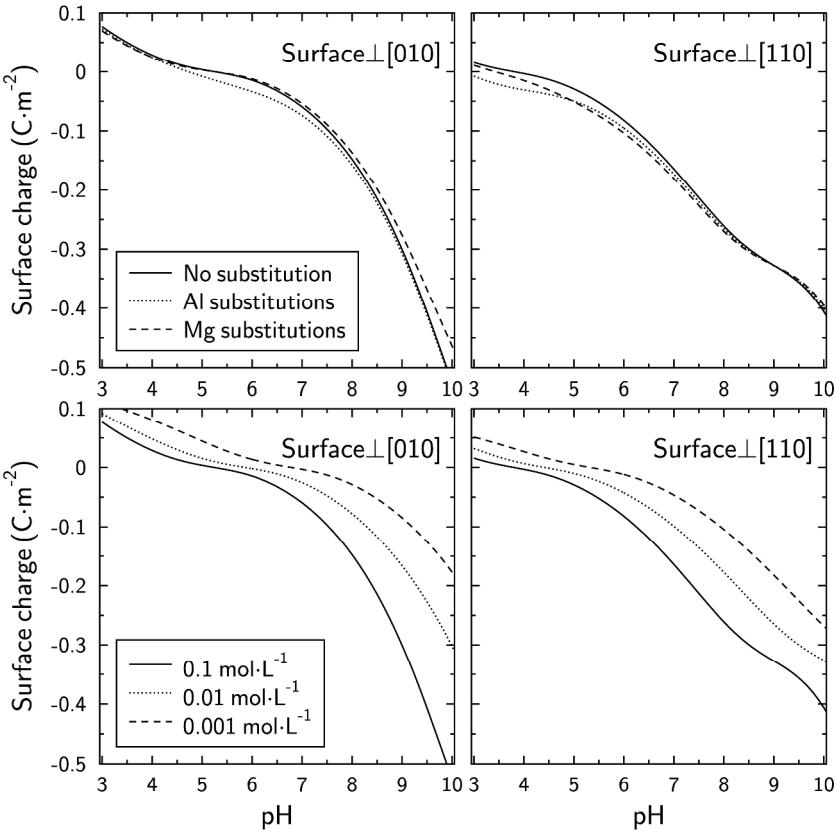

Figure 4

297x420mm (300 x 300 DPI)

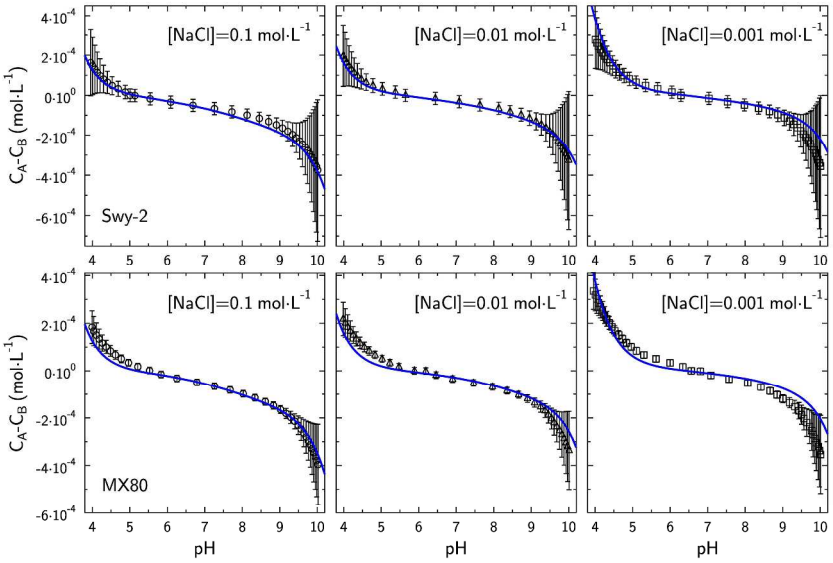

Figure 5

297x420mm (300 x 300 DPI)

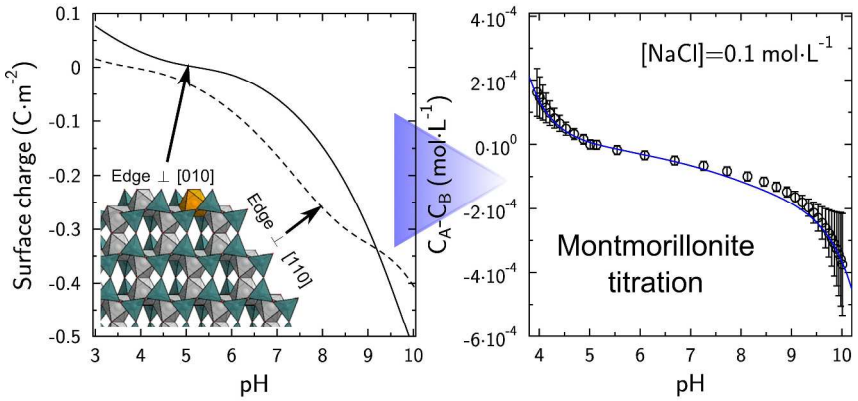

TOC

297x420mm (300 x 300 DPI)